Geophysical Research Letters

RESEARCH LETTER
10.1029/2019GL082826

Key Points:
- Diurnal turbulent flux variability in wintertime is evident over both the Kuroshio Extension and the Gulf Stream
- The diurnal flux is tightly tied to the location of the maximum surface fluxes along the western boundary currents
- Higher winds are associated with moister surface layer air, indicating surface fluxes, not entrainment mixing, are key to this process

Correspondence to:
C. A. Clayson,
cclayson@whoi.edu

Citation:
Clayson, C. A., & Edson, J. B. (2019). Diurnal surface flux variability over western boundary currents. *Geophysical Research Letters*, *46*, 9174–9182. https://doi.org/10.1029/2019GL082826

Received 13 MAR 2019
Accepted 15 JUL 2019
Accepted article online 17 JUL 2019
Published online 5 AUG 2019

Diurnal Surface Flux Variability Over Western Boundary Currents

Carol Anne Clayson[1] **and James B. Edson**[2]

[1]Physical Oceanography, Woods Hole Oceanographic Institution, Woods Hole, MA, USA, [2]Applied Ocean Physics and Engineering, Woods Hole Oceanographic Institution, Woods Hole, MA, USA

Abstract An analysis of a satellite ocean surface turbulent flux product demonstrated that, as expected, the western boundary current regions dominate the seasonal cycle amplitude. Surprisingly, our analysis of the global ocean diurnal flux variability also demonstrated a regional maximum in the winter over the western boundary current regions. We conducted comparisons with in situ data from several buoys located in these regions. The buoy data were in general agreement with the relative magnitude, timing, and importance of each of the bulk parameters driving the latent and sensible heat fluxes. Further analysis demonstrated that the strength and timing of the diurnal signal is related to the location of the buoy relative to the region of maximum heat flux and sea surface temperature gradient. In both regions, the timing of the higher winds coincides with the moistest surface layer, indicating that surface fluxes rather than entrainment mixing play a key role in this phenomenon.

Plain Language Summary The Gulf Stream and Kuroshio are perhaps the most well-known surface currents in the global ocean system, strongly affecting the weather and climate in the Atlantic and Pacific regions and the surrounding continents. The wintertime exchanges of heat and water between the ocean and atmosphere in these regions, often associated with storms, are some of the largest observed. They affect not only the strongly coupled local ocean and atmosphere but also large-scale weather systems. Understanding these linkages between the ocean and atmosphere is a key part of understanding the evolution of storms. These warm water, strong-current regions typically experience no wintertime daily warming of the upper ocean, as there is less sunlight and stronger winds during this season. As a result, no consistent daily change in the air temperature or the surface exchanges of heat is expected over this region. However, when we analyzed wintertime variability of the surface and lower atmosphere over these regions from satellite records, we found a consistent daily variability of the lower atmosphere. This result was verified by comparisons with buoys in the region. This unexpected result implies that there are some physical processes in the lower atmosphere that still remain for us to understand.

1. Introduction and Motivation

The western boundary current (WBC) systems in the Northern Hemisphere midlatitudes, the Gulf Stream (GS) and the Kuroshio Extension (KE), have become an increasingly important focus of weather and climate studies, as both are components of larger oceanic circulations (Hurrell et al., 2003; Yasuda, 2003). They play an important role in the large-scale transport of heat in the Northern Hemisphere (Trenberth & Caron, 2001; Trenberth & Fasullo, 2017). In addition, the WBCs are consistently the location for intense air-sea exchange, particularly in wintertime, as cold, dry continental air is advected over the intense sea surface temperature (SST) gradient to waters that can be warmer than the air by 15° or more, leading to heat fluxes on the order of 1,000 W/m^2 in the GS region (Kelly et al., 2010; Marshall et al., 2009). The WBC regions evidence the largest seasonal variability across the global oceans (e.g., Figure 1a).

The collocation of these large air-sea heat fluxes, the SST gradients, and the mid-latitude storm tracks (e.g., Small et al., 2014) combine to make the WBCs a hot spot for air-sea interaction across a variety of temporal scales, from individual storms to maintenance of mode water to multidecadal atmospheric circulation variability (Booth et al., 2012; Kwon et al., 2010; Marshall et al., 2009). As such, the mechanisms that contribute to the mean and transient structure of the atmospheric boundary layer and the coupling feedbacks between the ocean and atmosphere are currently a topic of much study. Numerous studies, including both observational and modeling, have demonstrated a tight coupling between surface winds and fluxes and the SST frontal

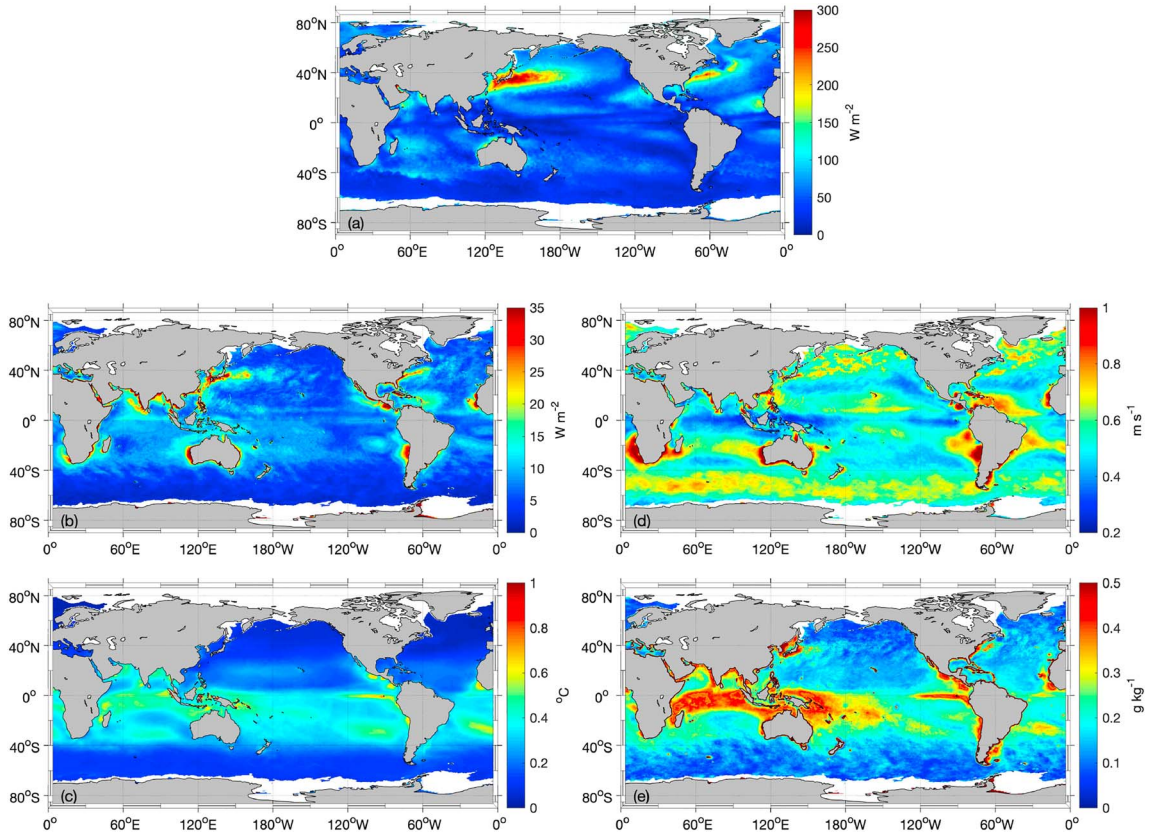

Figure 1. (a) Absolute value of the difference between the mean December-January-February (DJF) and the mean June-July-August latent heat flux. Also shown is the amplitude of the mean DJF diurnal variability of the latent heat flux (b), SST (c), wind speed (d), and air-sea specific humidity difference (e). Data are from satellite estimates (section 2.1).

zone (e.g., O'Neill et al., 2012; Plagge et al., 2016), but the mechanism (or mechanisms) by which the SST fronts influence the surface winds is still under debate (Small et al., 2008).

The importance of another natural mode of variability between the ocean and atmospheric across the global ocean is also receiving more attention, as the importance of diurnal variability in SST in driving a variety of phenomena from the convection scale (Slingo et al., 2003; Webster et al., 1996) to the intraseasonal (MJO) scale (e.g., Seo et al., 2014; Shinoda, 2005) to ENSO (Bernie et al., 2008). Clayson and Bogdanoff (2013) demonstrated the importance of including the diurnal SST variability in calculation of the climate mean air-sea fluxes, with the largest impact on mean air-sea fluxes occurring in the tropics. Diurnal SST-forced variability in the fluxes also occurred outside of the tropics, but the largest impacts were generally limited to summer months when solar insolation and SST variability is at a maximum.

In an analysis of satellite-based mean diurnal variability of the air-sea fluxes themselves, however, another maximum in latent heat flux diurnal variability outside of the tropics during austral-winter is also evident (Figure 1b). This diurnal variability is also evident in the sensible heat flux analysis (e.g., Figure 3) even though the mean diurnal warming is roughly 0 °C (Figure 1c). To determine whether this unexpected result is due to inaccuracies in the satellite fluxes, or a real but unreported phenomenon, this paper will explore comparisons of the satellite fluxes with available buoys in WBC regions, evaluate the variability as seen in the buoys as a function of location with respect to the WBC, and discuss the implications of the observations.

2. Data

2.1. Satellite Estimates

The satellite fluxes shown here use the SeaFlux-CDR (Climate Data Record) version 2 (Roberts et al., 2010; hereafter referred to as SeaFlux_v2). SeaFlux_v2 is based mainly on the Sensor Microwave/Imager and the Special Sensor Microwave/Imager Sounder instruments. The method for determining 10-m air temperature

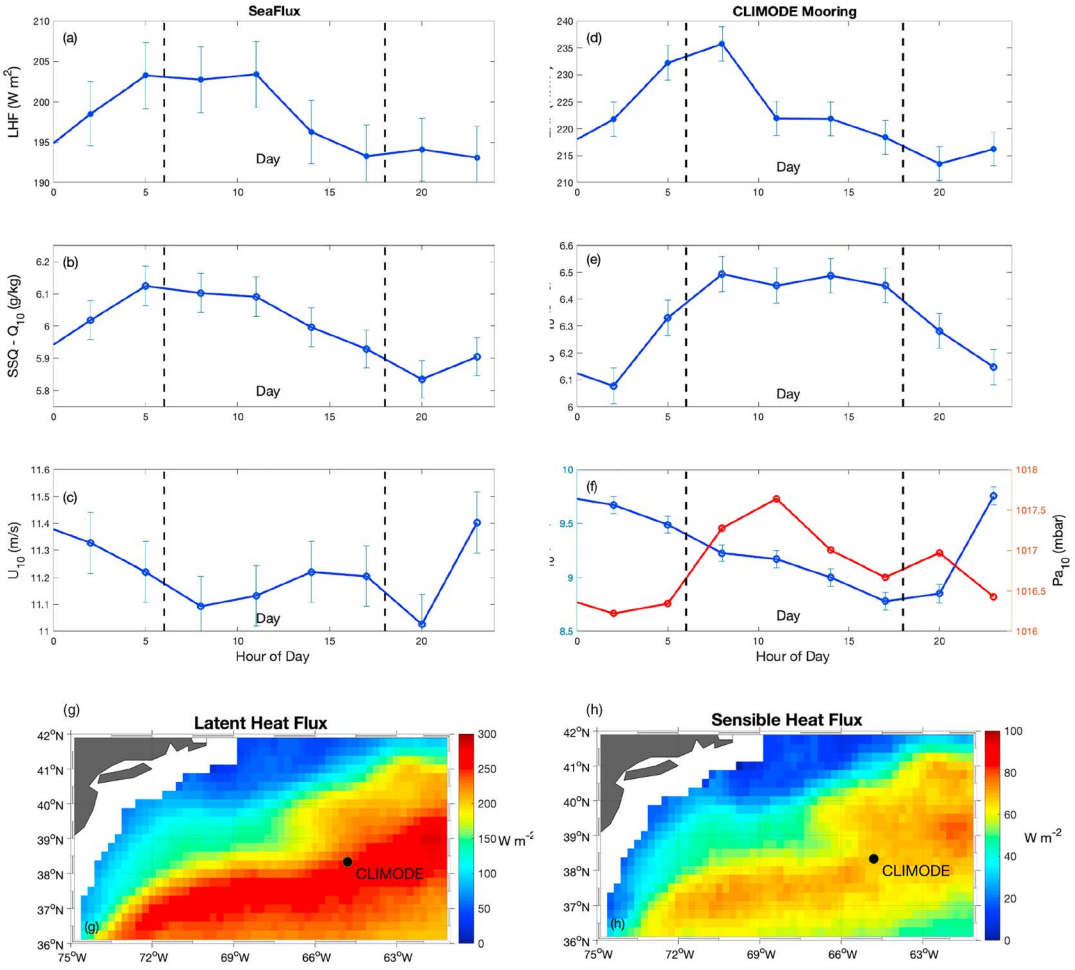

Figure 2. Diurnal cycles of latent heat flux (a, d), ΔQ (b, e), and U_{10} (c, f) and pressure (red) from SeaFlux_v2 (a–c) and CLIMODE mooring (d–f). Uncertainties are the observations standard error. Dashed vertical lines indicate sunrise/sunset. Also shown are the 5-month averages of latent (g) and sensible heat flux (h) from SeaFlux_v2 and the location of the CLIMODE mooring. Note the differing scales between satellite and buoy plots.

(T_{10}), specific humidity (Q_{10}), and wind speed (U_{10}) is based on the retrieval methodology of Roberts et al. (2010); all retrievals are combined and interpolated in space and time using bias-corrected MERRA values. The diurnal SST is based on a parameterization using satellite precipitation, radiation, and winds (as discussed in Clayson & Bogdanoff, 2013). The bulk fluxes are then calculated using COARE 3.0 (Fairall et al., 2003). The C-ATBD document describing the production of the inputs and fluxes (Clayson & Brown, 2016), code for this production, and the data set is available from the NOAA Climate Data Records repository from 1988—near present at 0.25° by 0.25° and 3-hourly resolution.

2.2. Buoy Observations

Buoy observations from the GS region of the North Atlantic are available from the sequence of buoys deployed during CLIMODE (CLIVAR Mode Water Dynamic Experiment, Marshall et al., 2009). The buoys were located at about 38.5°N, 65°W, and observations were made from the first CLIMODE buoy from 13 November 2005 through 19 November 2006 and the subsequent buoy from 20 November 2006 through 1 February 2007 (Weller et al., 2012). The buoy was located near and generally south of the northern wall of the GS except for periods when GS meanders placed it in shelf water. The buoys had redundant sensor packages including wind speed and direction, air temperature, relative humidity, pressure, and sea temperature. The buoy data have undergone extensive quality control (Bigorre et al., 2013) and are available as 1-min averages.

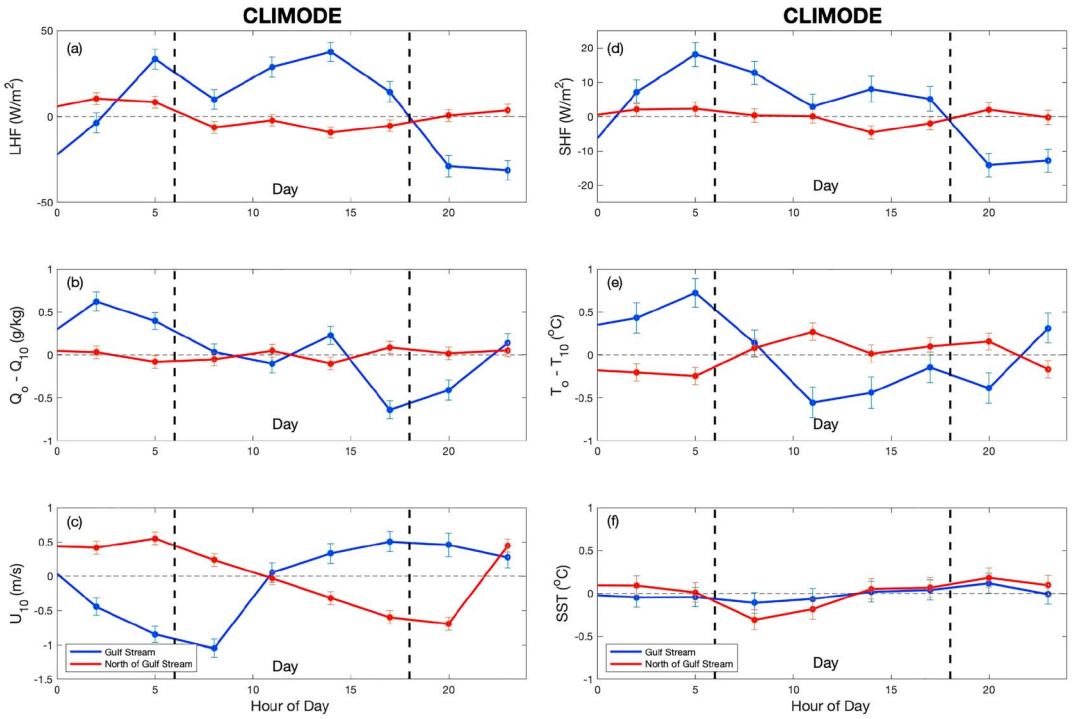

Figure 3. Comparison of diurnally averaged values of the LHF (a) and SHF (d), ΔQ (b), SST-T_{10} (e), U_{10} (c),and SST (f) from the CLIMODE mooring within the Gulf Stream (SST > 22.0 °C; shown in blue) versus north of the Gulf Stream (SST < 22.0 °C; shown in red). The means have been removed in these plots to improve comparison. The means are LHF GS: 305.2 W/m^2; LHF North: 188.8 W/m^2; ΔQ GS: 8.99 g/kg^1; ΔQ North: 5.61 g/kg^1; U_{10} GS: 10.83 m/s; and U_{10} North: 8.65 m/s. LHF = latent heat flux; SHF = sensible heat flux; SST = sea surface temperature.

Buoy observations from the KE region are available from two programs. The first is the Kuroshio Extension Observatory (KEO) series of buoy deployments, operating under the NOAA Ocean Climate Stations Project as part of the Ocean Sustained Interdisciplinary Time series Environmental Observatory (OceanSITES) network (Cronin et al., 2008). The KEO buoys are nominally located south of the KE current, at 32.3°N, 144.6°E, and have been delivering data from 16 June 2004 through the present. The second buoy near the KE is the JAMSTEC Kuroshio Extension Observatory (JKEO) buoy, which is also part of the OceanSITES network (Konda et al., 2010). The JKEO series of buoys were nominally located on the northern side of the KE current, at 38.0°N, 146.5°E. The JKEO buoy recorded data from roughly 18 February 2007 through 2 July 2013. Sustained buoy observations in the WBC regions remain a technological challenge; loss of sensors and data dropouts remains a factor in which time periods could be used for comparisons and analysis in this investigation. Both buoys measure winds, air and sea temperature, and specific humidity (among other meteorological and oceanographic measurements) as 10-min averages. The sensible heat flux (SHF) and latent heat flux (LHF) were calculated from all of the buoy-measured meteorological measurements using the COARE 3.5 algorithm (Edson et al., 2013) at the time of each measurement.

3. Methods

The Sea_Flux_v2 data are available every 3 hr at 00, 03, 06, 09, 12, 15, 18, and 21 GMT. In order to discern the diurnal signal, the mean and standard deviation of the SeaFlux_v2 data are computed at each of these times over the time period of interest (i.e., December-January-February). The maximum minus minimum values of this composite diurnal cycle across the globe are shown in Figures 1b and 1c. A similar methodology was used for the buoy analysis, with the exception that the higher resolution buoy data are binned over 3-hr intervals with bins centered at 00, 03, 06, 09, 12, 15, 18, and 21 GMT. A composite buoy diurnal cycle is then created by finding the median value within each 3-hr bin. All times shown are local times at the buoys.

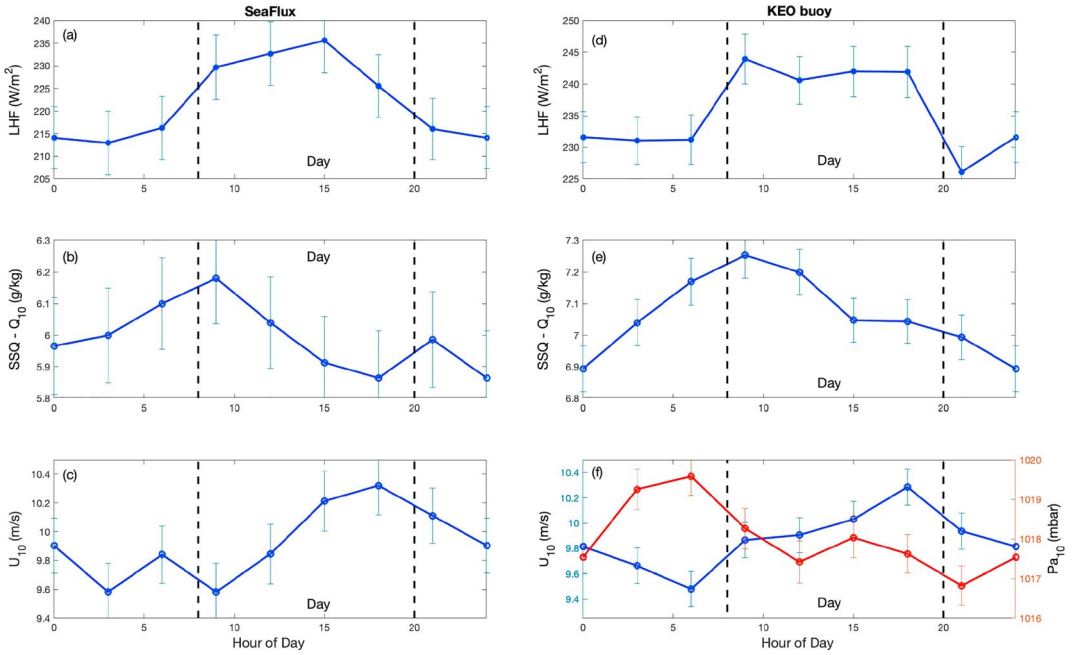

Figure 4. As in Figure 2 but for the KEO buoy location. Data are averaged over the time periods of December 2004 to February 2005; February 2007; and December 2007 to mid-February 2008. KEO = Kuroshio Extension Observatory; LHF = latent heat flux.

4. Results

4.1. GS diurnal cycle

As a way of validating the existence of the diurnal cycle seen in the wintertime satellite records, a comparison was performed for the 5 months of wintertime data available from the CLIMODE buoy: December 2005 to February 2006 and December 2006 to January 2007. The location of the CLIMODE buoy during these five winter months as compared to the average LHF and SHF is shown in Figure 2. The buoy is located near the maximum of the turbulent flux during this time period. The mean diurnal cycle from both the satellite data (taken from the grid point which includes the location of the buoy) and the CLIMODE buoy is also shown in Figure 2. The mean diurnal cycle in LHF as shown by the satellite is roughly 15 W/m^2, with a peak at the noon observation; the CLIMODE buoy also displays a diurnal cycle, with an even larger value of 20 W/m^2, also with a peak at the noon observation. In both the satellite and in situ data sets, there is a diurnal cycle evident in both the air-sea specific humidity difference (ΔQ, roughly 0.5 g/kg) and the wind speed (U_{10}, 0.4 m/s in the satellite data, 1.0 m/s in the buoy data). A diurnal cycle is also evident in the pressure signal that is out of phase with the wind speed. The anticorrelation is consistent with observations and model studies of thermally direct circulations (see Small et al., 2008) producing higher winds (lower pressure) over warm water and lower winds (higher pressure) over cold (e.g., Chelton et al., 2001; O'Neill et al., 2010; Plagge et al., 2016). However, the absence of a diurnal cycle in SST implies that the circulation must be driven by another, possibly related, mechanism.

Differences between the satellite and buoy data may be due to the much larger footprint of the satellite data, which tends to smear out the sharp SST gradients and possibly the resulting boundary layer characteristics (e.g., Skyllingstad & Edson, 2009). In addition, the satellite data background ΔQ is less than the observed; this could be related to the known underestimation of the satellite humidity at larger ΔQ (e.g., Bentamy et al., 2017; Clayson & Brown, 2016). There is similarity in the timing of the peak ΔQ and U_{10} between the satellite and in situ data; ΔQ peaks during the daytime hours, and U_{10} peaks in the hours just after midnight.

Given that both data sets evidence a diurnal cycle in the LHF, ΔQ, and wind speed, we now investigate the features of the diurnal cycle that can be observed in the buoy data. There is a minimum in ΔQ in the pre-

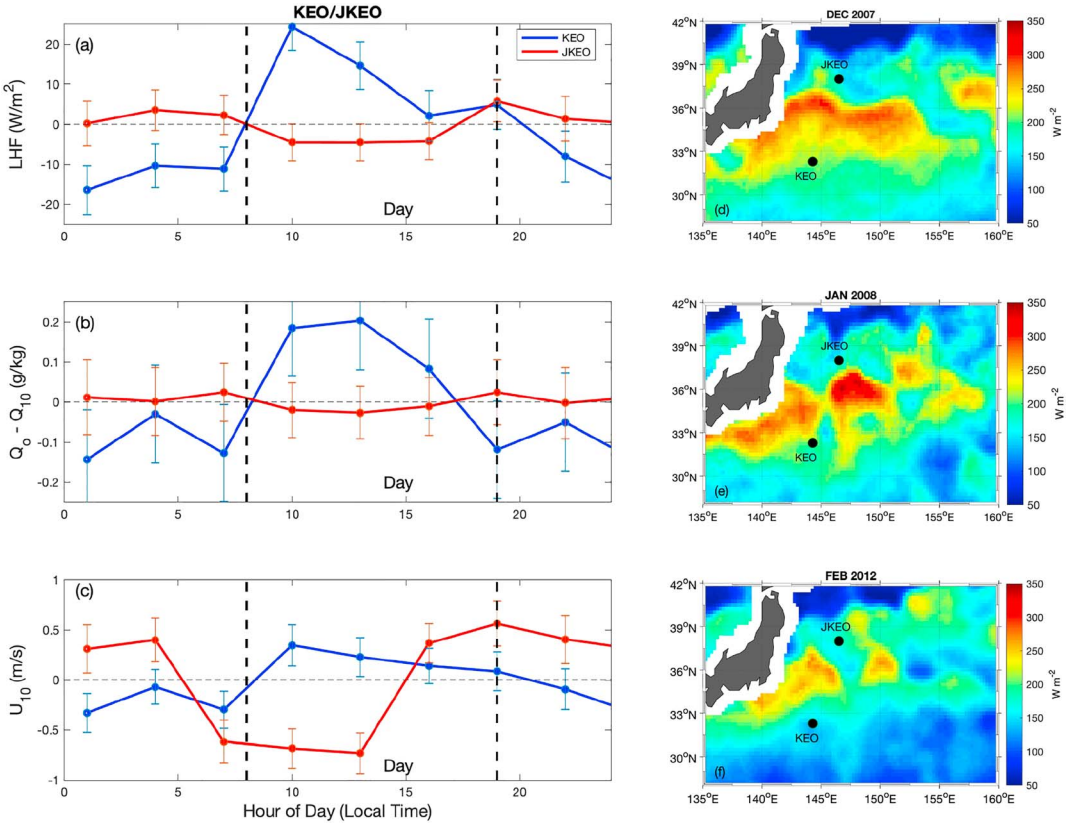

Figure 5. Perturbations in (a) LHF, (b) ΔQ, and (c) U_{10} about their respective means at the KEO (blue) and JKEO (red) buoy locations. Buoy locations and the average LHF fluxes for the three comparison winter months are shown in (d) to (f). The means are LHF KEO: 240.0 W/m^2; LHF JKEO: 175.7 W/m^2; ΔQ KEO: 7.26 g/kg; ΔQ JKEO: 5.57 g/kg; U_{10} KEO: 9.94 m/s; and U_{10} JKEO: 8.02 m/s. JKEO = JAMSTEC Kuroshio Extension Observatory; KEO = Kuroshio Extension Observatory; LHF = latent heat flux; SHF = sensible heat flux; SST = sea surface temperature.

dawn hours, followed by a maximum during the day. As there is no diurnal SST and thereby no diurnal ΔQ cycle during these months as shown in Figure 3f, this cycle is determined by the atmospheric humidity, meaning that the near surface boundary layer is moister during the nighttime and drier during the daytime. Conversely, the winds are elevated at nighttime and begin decreasing during the early morning hours. The combination of these two timings produces a peak in the latent heat flux near the middle of the daytime.

Results from the satellite spatial analysis indicate that the diurnal cycle is fairly restricted to the region of the maximum heat flux associated with the GS. To investigate the importance of the location of the observations, the data from the CLIMODE buoy are divided between time periods when the buoy is in the GS (SST > 22.0 °C; ~31 days) and when it is just north of the GS (SST < 22.0 °C; ~84 days). The associated composite cycles are shown in Figure 3. When the buoy is in the GS itself, the diurnal cycle of LHF and SHF is considerably stronger than the 5-month composite, with peaks of nearly 40 W/m^2 greater during the daytime than the nighttime. When the buoy is north of the GS, the mean fluxes are much lower, and the diurnal cycle is less distinct and reduced in scale (<20 W/m^2). This reduction is true of both the humidity and wind fields. The near surface GS boundary layer is drier by more than 1 g/kg in the early morning and daytime hours than later in the evening/night, and the wind speed drops in the early daytime period by almost 2 m/s. Also as compared to the 5-month composite, there is less ascynchronicity of the humidity and winds; the driest boundary layer occurs roughly during the same hours as the lowest wind speeds.

North of the GS, there is still a diurnal cycle in winds, although the scale is half of that seen in the GS, and is 180° out of phase. There is no discernable coherent cycle in the moisture fields or in the resulting latent heat flux. The phenomenon as shown by the in situ data appears to be confined to the local GS boundary layer, as

evidenced in the satellite data as well. It should also be noted that the overall mean wind speeds during the entire averaging period give lower (higher) wind speeds over colder (warmer) water, which is consistent with previous studies as noted above.

4.2. KE diurnal cycle

The satellite data demonstrated that the observed diurnal cycle was not limited to the GS but was also evident near the KE. The KEO and JKEO buoys can be compared with the CLIMODE buoy, with each other, and over several years. However, as noted above, there are significant time periods during the winter months when data are unavailable from either the JKEO or KEO buoy. As well, there is interannual variability in the strength and location of the KE and its relation to these buoys (Figure 5).

During years near the CLIMODE observation time, which also coincide with the KEO buoy located closest to the peak of the LHF, there are roughly 7.5 months for comparison between the satellite data and the KEO buoy data as shown in Figure 4. The general diurnal cycle in LHF, ΔQ, and U_{10} are similar between the two data sets. As with the CLIMODE comparisons, the U_{10} diurnal cycle is somewhat reduced in the satellite data set, and the mean of the ΔQ diurnal cycle is also shifted lower. This leads to a smaller diurnal cycle in the satellite LHF (~15 W/m^2 as compared to 25 W/m^2). However, the timings of the peaks in the cycle are similar between the satellite and buoy data sets, with drier air occurring during the morning hours with peak wind speeds occurring in the afternoon.

As occurred in the GS, observations from the north side of the Kuroshio Extension show reduced overall LHF, and little diurnal cycle in ΔQ and LFH, with still a significant diurnal cycle in the winds (Figure 5). The data are averaged over the only winter months when both buoys had data: December 2007, January 2008, and February 2012. In February 2012 the KEO buoy was located even further south of the also-reduced latent heat than the months included in Figure 4, also in contrast to the CLIMODE buoy. Comparing the cycles measured on the buoys during these 3 months in Figure 5 demonstrates a difference in the timing of the diurnal cycle and perhaps a decoupling of the higher winds/moister boundary layer relationship when the observations are made well south of the KE. This is in contrast to the results shown in Figures 2 and 4, where the observations are more consistently within or just north of the WBC.

5. Conclusions

Satellite and in situ observations from both the GS and KE regions demonstrated cohesive diurnal variability in winds, humidity, temperature, LHF, and SHF. The strength and timing of this diurnal variability depends on the location relative to the heat flux maxima over the WBC. The strength of the mean CLIMODE buoy cycle (~23 W/m^2) was stronger than the KEO buoy (~18 W/m^2), possibly due to the CLIMODE buoy being nearer the peak latent heat flux region. At both locations, the driest air tends to occur in the early morning hours; the timing of the minimum wind speed differs somewhat between the two locations. This leads to differences in timing of the LHF maximum. In agreement with numerous previous studies (e.g., Chelton et al., 2001; O'Neill et al., 2010; Plagge et al., 2016), the mean winds are slower (faster) over cooler (warmer) water on either side of the SST front as reported by the captions in Figures 4 and 5. The diurnal variability identified in this study is in addition to this spatial pattern.

In both regions, north of the WBC there is still a significant (~1 m/s) coherent diurnal cycle in the winds, but no coherent diurnal cycle exists in specific humidity. The ubiquity of the diurnal wind cycle would be consistent with previous observations of general diurnal wind features over the global oceans during the winter months (e.g., Dai & Deser, 1997). However, the diurnal cycle in humidity seems to be tied very strongly to the location of the SST front and resulting heat flux maxima. At both locations the drier near surface boundary layer air tends to occur with lower winds, although there is a lag between the cycling. This provides a key to a possible local mechanism for the diurnal cycle. Two possibilities include entrainment mixing and forcing by surface fluxes. If entrainment mixing were the key to this process, higher winds are expected to be associated with a drier boundary layer due to entrainment of dry air from aloft. However, since the higher winds are associated with a moister surface layer, it is more likely that the surface fluxes are a key to this phenomenon as the higher winds help drive a higher latent heat flux, which then leads to moistening of the boundary layer. Given that this is the first set of observations showing this wintertime diurnal variability, further work is necessary to fully establish the statistics and mechanisms of

the processes involved. As the satellite data show similar qualitative response to the buoy data, it may be a useful tool for further exploration.

Acknowledgments
CAC gratefully acknowledges funding from the NASA MAP and NEWS programs (NNX13AN48G and NNX15AI47A). CLIMODE data were funded by the U.S. National Science Foundation (http://uop.whoi.edu/projects/CLIMODE/climodedata.html). KEO data are provided by the OCS Project Office of NOAA/PMEL (https://www.pmel.noaa.gov/ocs/data/disdel/). JKEO data are provided by RIGC/JAMSTEC and PMEL/NOAA (http://www.jamstec.go.jp/iorgc/ocorp/ktsfg/data/jkeo/). SeaFlux data are provided by the U.S. NOAA Climate Data Record Program (https://www.ncdc.noaa.gov/cdr).

References

Bentamy, A., Piollé, J. F., Grouazel, A., Danielson, R., Gulev, S., Paul, F., et al. (2017). Review and assessment of latent and sensible heat flux accuracy over the global oceans. *Remote Sensing of Environment*, *201*, 196–218.

Bernie, D., Guilyardi, E., Madec, G., Slingo, J., Woolnough, S., & Cole, J. (2008). Impact of resolving the diurnal cycle in an ocean-atmosphere GCM. Part 2: A diurnally coupled CGCM. *Climate Dynamics*, *31*(7–8), 909–925. https://doi.org/10.1007/s00382-008-0429-z

Bigorre, S. P., Weller, R. A., Edson, J. B., & Ware, J. D. (2013). A surface mooring for air-sea interaction research in the Gulf Stream. Part II: Analysis of the observations and their accuracies. *Journal of Atmospheric and Oceanic Technology*, *30*(3), 450–469. https://doi.org/10.1175/JTECH-D-12-00078.1

Booth, J. F., Thompson, L., Patoux, J., & Kelly, K. A. (2012). Sensitivity of midlatitude storm intensification to perturbations in the sea surface temperature near the Gulf Stream. *Monthly Weather Review*, *140*(4), 1241–1256. https://doi.org/10.1175/MWR-D-11-00195.1

Chelton, D. B., Esbensen, S. K., Schlax, M. G., Thum, N., Freilich, M. H., Wentz, F. J., et al. (2001). Observations of coupling between surface wind stress and sea surface temperature in the eastern tropical Pacific. *Journal of Climate*, *14*(7), 1479–1498. https://doi.org/10.1175/1520-0442(2001)014<1479:OOCBSW>2.0.CO;2

Clayson, C. A., & Bogdanoff, A. (2013). The effect of diurnal sea surface temperature warming on climatological air-sea fluxes. *Journal of Climate*, *26*(8), 2546–2556. https://doi.org/10.1175/JCLI-D-12-00062.1

Clayson, C. A. & Brown, J. (2016). NOAA Climate Data Record Ocean Surface Bundle (OSB) Climate Data Record (CDR) of Ocean Heat Fluxes, Version 2. Climate Algorithm Theoretical Basis Document (C-ATBD), NOAA National Center for Environmental Information. https://doi.org/10.7289/V59K4885.

Cronin, M. F., Meinig, C., Sabine, C. L., Ichikawa, H., & Tomita, H. (2008). Surface mooring network in the Kuroshio Extension. *IEEE Systems Special Issue on GEOSS*, *2*(3), 424–430. https://doi.org/10.1109/JSYST.2008.925982

Dai, A., & Deser, C. (1997). Diurnal and semidiurnal variations in global surface wind and divergence fields. *Journal of Geophysical Research*, *104*, 31,109–31,125.

Edson, J. B., Jampana, V., Weller, R. A., Bigorre, S. P., Plueddemann, A. J., Fairall, C. W., et al. (2013). On the exchange of momentum over the open ocean. *Journal of Physical Oceanography*, *43*(8), 1589–1610. https://doi.org/10.1175/JPO-D-12-0173.1

Fairall, C. W., Bradley, E. F., Hare, J. E., Grachev, A. A., & Edson, J. B. (2003). Bulk parameterization of air-sea fluxes: Updates and verification for the COARE algorithm. *Journal of Climate*, *16*(4), 571–591. https://doi.org/10.1175/1520-0442(2003)016<0571:BPOASF>2.0.CO;2

Hurrell, J. W., Kushnir, Y., Ottersen, G., & Visbeck, M. (2003). *An overview of the North Atlantic Oscillation. The North Atlantic Oscillation, Geophysical Monograph*, *American Geophysical Union* (Vol. 134, pp. 1–35).

Kelly, K. A., Small, R. J., Samelson, R. M., Qiu, B., Joyce, T. M., Kwon, Y., & Cronin, M. F. (2010). Western boundary currents and frontal air-sea interaction: Gulf Stream and Kuroshio Extension. *Journal of Climate*, *23*(21), 5644–5667. https://doi.org/10.1175/2010JCLI3346.1

Konda, M., Ichikawa, H., Tomita, H., & Cronin, M. F. (2010). Surface heat flux variations across the Kuroshio Extension as observed by surface flux buoys. *Journal of Climate*, *23*(19), 5206–5221. https://doi.org/10.1175/2010JCLI3391.1

Kwon, Y., Alexander, M. A., Bond, N. A., Frankignoul, C., Nakamura, H., Qiu, B., & Thompson, L. A. (2010). Role of the Gulf Stream and Kuroshio-Oyashio systems in large-scale atmosphere-ocean interaction: A review. *Journal of Climate*, *23*(12), 3249–3281. https://doi.org/10.1175/2010JCLI3343.1

Marshall, J., Ferrari, R., Forget, G., Maze, G., Andersson, A., Bates, N., et al. (2009). The Climode Field Campaign: Observing the cycle of convection and restratification over the Gulf Stream. *Bulletin of the American Meteorological Society*, *90*, 1337–1350.

O'Neill, L. W., Chelton, D. B., & Esbensen, S. K. (2010). The effects of SST-induced surface wind speed and direction gradients on midlatitude surface vorticity and divergence. *Journal of Climate*, *23*(2), 255–281. https://doi.org/10.1177/2009JCLI2613.1

O'Neill, L. W., Chelton, D. B., & Esbensen, S. K. (2012). Covariability of surface wind and stress responses to sea surface temperature fronts. *Journal of Climate*, *25*(17), 5916–5942. https://doi.org/10.1175/JCLI-D-11-00230.1

Plagge, A., Edson, J. B., & Vandemark, D. (2016). In situ and satellite evaluation of air-sea flux variation near ocean temperature gradients. *Journal of Climate*, *29*(4), 1583–1602. https://doi.org/10.1175/JCLI-D-15-0489.1

Roberts, J. B., Clayson, C. A., Robertson, F. R., & Jackson, D. L. (2010). Predicting near-surface characteristics from Special Sensor Microwave/Imager using neural networks with a first-guess approach. *Journal of Geophysical Research*, *115*, D19113. https://doi.org/10.1029/2009JD013099

Seo, H., Subramanian, A. C., Miller, A. J., & Cavanaugh, N. R. (2014). Coupled impacts of the diurnal cycle of sea surface temperature on the Madden-Julian Oscillation. *Journal of Climate*, *27*(22), 8422–8443. https://doi.org/10.1175/JCLI-D-14-00141.1

Shinoda, T. (2005). Impact of diurnal cycle of solar radiation on intraseasonal SST variability in the western equatorial Pacific. *Journal of Climate*, *18*(14), 2628–2636. https://doi.org/10.1175/JCLI3432.1

Skyllingstad, E. D., & Edson, J. B. (2009). Large-eddy simulation of moist convection during a cold-air outbreak over the Gulf Stream. *Journal of the Atmospheric Sciences*, *66*(5), 1274–1293. https://doi.org/10.1175/2008JAS2755

Slingo, J. M., Inness, P., Neale, R., Woolnough, S., & Yang, G. Y. (2003). Scale interactions on diurnal to seasonal timescales and their relevance to model systematic errors. *Annals of Geophysics*, *46*, 139–155.

Small, R. J., deSzoeke, S. P., Xie, S. P., O'Neill, L., Seo, H., Song, Q., et al. (2008). Air-sea interaction over ocean fronts and eddies. *Dynamics of Atmospheres and Oceans*, *45*(3-4), 274–319. https://doi.org/10.1016/j.dynatmoce.2008.01.001

Small, R. J., Tomas, R. A., & Bryan, F. O. (2014). Storm track response to ocean fronts in a global high-resolution climate model. *Climate Dynamics*, *43*(3-4), 805–828. https://doi.org/10.1007/s00382-013-1980-9

Trenberth, K. E., & Caron, J. M. (2001). Estimates of meridional atmosphere and ocean heat transports. *Journal of Climate*, *14*(16), 3433–3443. https://doi.org/10.1175/1520-0442(2001)014<3433:EOMAAO>2.0.CO;2

Trenberth, K. E., & Fasullo, J. T. (2017). Atlantic meridional heat transports computed from balancing Earth's energy locally. *Geophysical Research Letters*, *44*, 1919–1927. https://doi.org/10.1002/2016GL072475

Webster, P. J., Clayson, C. A., & Curry, J. A. (1996). Clouds, radiation, and the diurnal cycle of sea surface temperature in the tropical western Pacific. *Journal of Climate*, *9*(8), 1712–1730. https://doi.org/10.1175/1520-0442(1996)009<1712:CRATDC>2.0.CO;2

Weller, R. A., Bigorre, S. P., Lord, J., Ware, J. D., & Edson, J. B. (2012). A surface mooring for air-sea interaction research in the Gulf Stream. Part I: Mooring design and instrumentation. *Journal of Atmospheric and Oceanic Technology*, *29*(9), 1363–1376. https://doi.org/10.1175/JTECH-D-12-00060.1

Yasuda, I. (2003). Hydrographic structure and variability in the Kuroshio-Oyashio transition area. *Journal of Oceanography*, *59*(4), 389–402. https://doi.org/10.1023/A:1025580313836